# SAR TOMOGRAPHY FOR SPATIO-TEMPORAL INVERSION OF POINT-LIKE SCATTERERS IN URBAN AREAS

*Muhammad A. Siddique*[1], *Urs Wegmüller*[2], *Irena Hajnsek*[1,3], *Othmar Frey*[1,2]

[1]Earth Observation and Remote Sensing, ETH Zurich, Switzerland
[2]Gamma Remote Sensing AG, Gümligen, Switzerland
[3]Microwaves and Radar Institute, German Aerospace Center - DLR, Oberpfaffenhofen, Germany

## ABSTRACT

Persistent scatterer interferometry (PSI) assumes the presence of a single temporally coherent scatterer in a range-azimuth pixel. Multiple scatterers interfering in the same pixel, as for the case of a layover, are typically rejected. Conventional SAR tomography (3D SAR) is a means to separate the individual scatterers in layover. Advanced tomographic inversion approaches employing extended phase models additionally allow simultaneous retrieval of scatterer elevation and deformation parameters. In this way, SAR tomography can increase deformation sampling and thereby complement a PSI-based analysis. This paper investigates the use of tomography as an add-on to PSI for spatio-temporal inversion of single and double scatterers in urban areas. Results are provided on an interferometric stack of 50 stripmap TerraSAR-X images acquired over the city of Barcelona.

***Index Terms—*** SAR tomography, persistent scatterer interferometry, multi-baseline interferometry, TerraSAR-X

## 1. INTRODUCTION

Persistent scatterer interferometry (PSI) [1, 2] is a state-of-the-art radar remote sensing technique for deformation analysis. In general, PSI-based approaches assume that a given range-azimuth pixel contains a single *point-like* scatterer exhibiting high temporal coherence – the so-called *persistent* scatterer. Pixels containing echoes from multiple scatterers, as in the case of a layover, are typically rejected. Urban areas are characterized by various man-made structures that tend to behave as point-like scatterers, but at the same time, layovers are frequent. The ability of SAR tomography to resolve scatterers in layover motivates its use as an extension to PSI. It is an aperture-synthesis approach which allows for separation of the interfering scatterers along the elevation (perpendicular to line-of-sight direction), as demonstrated in different investigations, such as [3, 4, 5]. The phase model conventionally associated with SAR tomographic inversion assumes a stationary scatterer and does not account for phase variations due to the deformation and/or dilation of the scatterer(s). Uncompensated phase variations lead to poor scatterer detection [6, 7]. SAR tomography with extended phase models [6, 8, 9, 10] allows modelling these variations, thereby not only improving scatterer detection but at the same time, allowing a simultaneous retrieval of the unknown scatterer elevation and deformation parameters.

This research project has been funded by the Swiss Space Office, State Secretariat for Education and Research of the Swiss Confederation (SER/SSO), via the MdP2012 initiative.

The processing steps employed in this work are the following. First, we perform a PSI analysis using the Interferometric Point Target Analysis (IPTA) framework [2] on an interferometric data stack of 50 stripmap TerraSAR-X images. A set of persistent scatterer (PS) candidate points is identified on the basis of high temporal stability of the backscattering and low spectral diversity. The data stack is phase calibrated and an atmospheric phase screen (APS) is iteratively isolated. For details, the reader is referred to [2, 11]. Once a reasonable PSI solution is obtained, the point-wise APS is extrapolated to nearby non-PS pixels. As a next step, we implement SAR tomography with three different phase models on all pixels (including those rejected by IPTA, which potentially include double-scatterers). The tomographic inversion is applied independently of the PSI solution, except that the same reference layer and reference point are used to allow for a subsequent consistency analysis, and that the baselines and the reference local temperatures used are also the same, as refined in the IPTA pre-processing. A generalized likelihood ratio test (GLRT), as proposed in [12], is employed next for the detection of single and double scatterers.

## 2. TOMOGRAHIC INVERSION

For a stable point target source, assuming no noise terms, the mathematical model for SAR tomography can be concisely written as [6, 9]:

$$y_n = \int_{\triangle \mathbf{p}} \gamma(\mathbf{p}) \exp\left[-j\varphi_n(\mathbf{p})\right] \mathrm{d}\mathbf{p} \tag{1}$$

where $y_n$ is the $n^{th}$ single-look-complex (SLC) pixel value from a coregistered interferometric stack containing $N$ images, $n = 0, 1, \ldots N-1$, $\gamma(\mathbf{p})$ and $\varphi_n(\mathbf{p})$ are the target reflectivity and interferometric phase, respectively, as a function of the unknown parameter vector $\mathbf{p}$. $\Delta\mathbf{p}$ represents the limits of integration for the unknown parameters. In case of conventional SAR tomography (3D-SAR), which assumes the scatterer(s) to be stationary, the interferometric phase is modelled as follows:

$$\varphi_n(\mathbf{p}) = 2k \triangle r_n(s) \tag{2}$$

where $s$ is the elevation, $\mathbf{p} = [s]$, and $\triangle r_n(s)$ is the sensor-to-target path-length difference for the interferometric pair:

$$\triangle r_n(s) = r_n(s) - r_0(s) \approx \frac{s^2}{2\left(r_0 - b_n^{\parallel}\right)} - \frac{b_n^{\perp} s}{r_0 - b_n^{\parallel}}. \tag{3}$$

$r_n$ is the range distance from sensor *n* to scatterer at elevation *s*, and $b_n^{\perp}$ and $b_n^{\parallel}$ represent the orthogonal and parallel components of the

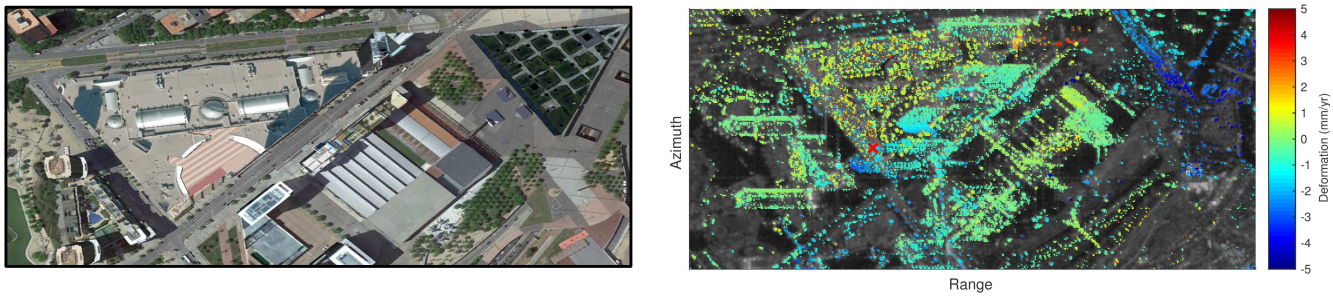


**Fig. 1**. Left: Google Earth snapshot of the observed urban area (Diagonal Mar, Barcelona). Right: An averaged intensity image of TerraSAR-X stack overlaid with dots marking the location of the persistent scatterers identified in the IPTA processing; the color of the dots represents the average deformation velocity as estimated with IPTA. The interferometric phase model used in the IPTA processing takes into account both a linear deformation over time as well as thermal dilation [13].

spatial baseline extended by sensor *n*, respectively. Here we consider $n = 0$ as the reference acquisition in the interferometric stack. This phase model is referred to as P1 onwards.

In case the scatterer is undergoing some motion, there are additional phase variations which need to be modelled. Assuming that the motion is a displacement within the same range pixel, differential SAR tomography [8, 12, 14] allows modelling it as a temporally linear deformation by extending the phase model as follows (referred to as P2 onwards):

$$\varphi_n(\mathbf{p}) = 2k\left[\triangle r_n(s) + \nu t_n\right] \tag{4}$$

where $\nu$ is the average deformation velocity, $t_n$ represents the temporal baselines, and $\mathbf{p} = [s, \nu]$ in this case. As shown in some recent PSI studies (such as [15][13]), the scatterer motion may partly be temperature-dependent, i.e. thermal dilation. Considering that the thermal dilation of building structures is linearly dependent on temperature, we extend P2 with a phase-to-temperature sensitivity term, $\kappa$, as given below:

$$\varphi_n(\mathbf{p}) = 2k\left[\triangle r_n(s) + \nu t_n + \frac{1}{2k}\kappa\tau_n\right] \tag{5}$$

with $\mathbf{p} = [s, \nu, \kappa]$ now, while $\tau_n$ is the $n^{th}$ temperature baseline, i.e. the difference between the local temperature at the time of the $n^{th}$ acquisition and the reference. This extended phase model is referred to as P3 onwards.

## 3. PARAMETER ESTIMATION & SCATTERER DETECTION

Different methods [4, 16] have been proposed for the inversion of the aforementioned tomographic models and the estimation of the unknown scatterer parameters. In this work we use the conventional single-look beamforming; the estimated reflectivity is given by

$$\hat{\gamma}(\mathbf{p}) = \mathbf{a}^H(\mathbf{p})\,\mathbf{y} \tag{6}$$

where $\mathbf{y}$ is the SLC vector and $\mathbf{a}(\mathbf{p})$ is the steering vector as a function of the unknown parameter vector $\mathbf{p}$:

$$\mathbf{a}(\mathbf{p}) = \left[\begin{array}{cccc} 1 & e^{-j\varphi_1(\mathbf{p})} & \ldots & e^{-j\varphi_{N-1}(\mathbf{p})} \end{array}\right]^{\mathrm{T}}. \tag{7}$$

For each of the three phase models discussed previously, an estimate of the parameter vector is computed by using the estimated reflectivity as the objective function in the following optimization:

$$\hat{\mathbf{p}}_1 = \arg\max_{\mathbf{p}} \left(\frac{1}{N}\frac{|\hat{\gamma}(\mathbf{p})|^2}{\|\mathbf{y}\|^2}\right). \tag{8}$$

This optimization allows estimating the parameters for a single-scatterer ($\hat{\mathbf{p}}_1$), since it is a global maximization. In order to detect the presence of two scatterers (at maximum) in the same pixel, or to assert the absence of any coherent scatterer, we use the *sequential generalized likelihood ratio test with cancellation* (SGLRTC), as proposed in [12], to distinguish between three hypothesis: $\mathcal{H}_0$, $\mathcal{H}_1$, and $\mathcal{H}_2$ (as noise only, single scatterer, or double scatterer, respectively).

$$\mathcal{H}_0 : \mathbf{y} = \mathbf{n} \tag{9}$$

$$\mathcal{H}_1 : \mathbf{y} = \gamma(\mathbf{p}_1)\,\mathbf{a}(\mathbf{p}_1) + \mathbf{n} \tag{10}$$

$$\mathcal{H}_2 : \mathbf{y} = \gamma(\mathbf{p}_1)\,\mathbf{a}(\mathbf{p}_1) + \gamma(\mathbf{p}_2)\,\mathbf{a}(\mathbf{p}_2) + \mathbf{n} \tag{11}$$

where $\mathbf{n}$ is the random noise vector, generally assumed to be zero-mean circular Gaussian. We avoid detailing here the theoretical exposition of SGLRTC, which is referred to [12]. In principle, the proposed test is implemented in two steps. Using the estimate $\hat{\mathbf{p}}_1$ and ignoring the presence of a possible second scatterer, the contribution of the first scatterer is subtracted (or *cancelled*) from the SLC vector. As a next step, a second beamforming-based global optimization is applied on the residue after the cancellation to estimate the unknown parameter vector of a potential second scatterer, i.e. $\mathbf{p}_2$.

$$\hat{\mathbf{p}}_2 = \arg\max_{\mathbf{p}} \left(\frac{|\mathbf{y}^H\hat{\mathbf{P}}_1^{\perp}\mathbf{a}(\mathbf{p})|}{\|\hat{\mathbf{P}}_1^{\perp}\mathbf{a}(\mathbf{p})\|\,\|\mathbf{y}\|}\right) \tag{12}$$

where

$$\hat{\mathbf{P}}_1^{\perp} = \mathbf{I}_N - \frac{\mathbf{a}(\hat{\mathbf{p}}_1)\,\mathbf{a}^H(\hat{\mathbf{p}}_1)}{N}. \tag{13}$$

The decision whether the pixel has a double-scatterer ($\mathcal{H}_2$) or otherwise ($\bar{\mathcal{H}}_2$) is made as follows [12]:

$$\left(\frac{\left|\mathbf{u}_c^H\mathbf{y}_c\right|^2}{\|\mathbf{y}_c\|^2}\right) \underset{\bar{\mathcal{H}}_2}{\overset{\mathcal{H}_2}{\gtrless}} T_2 \tag{14}$$

where $\mathbf{u}_c = \hat{\mathbf{P}}_1^{\perp}\mathbf{a}(\hat{\mathbf{p}}_2)/\|\hat{\mathbf{P}}_1^{\perp}\mathbf{a}(\hat{\mathbf{p}}_2)\|$ and $\mathbf{y}_c = \hat{\mathbf{P}}_1^{\perp}\mathbf{y}$. In case the hypothesis $\mathcal{H}_2$ is rejected, a second decision is made next between

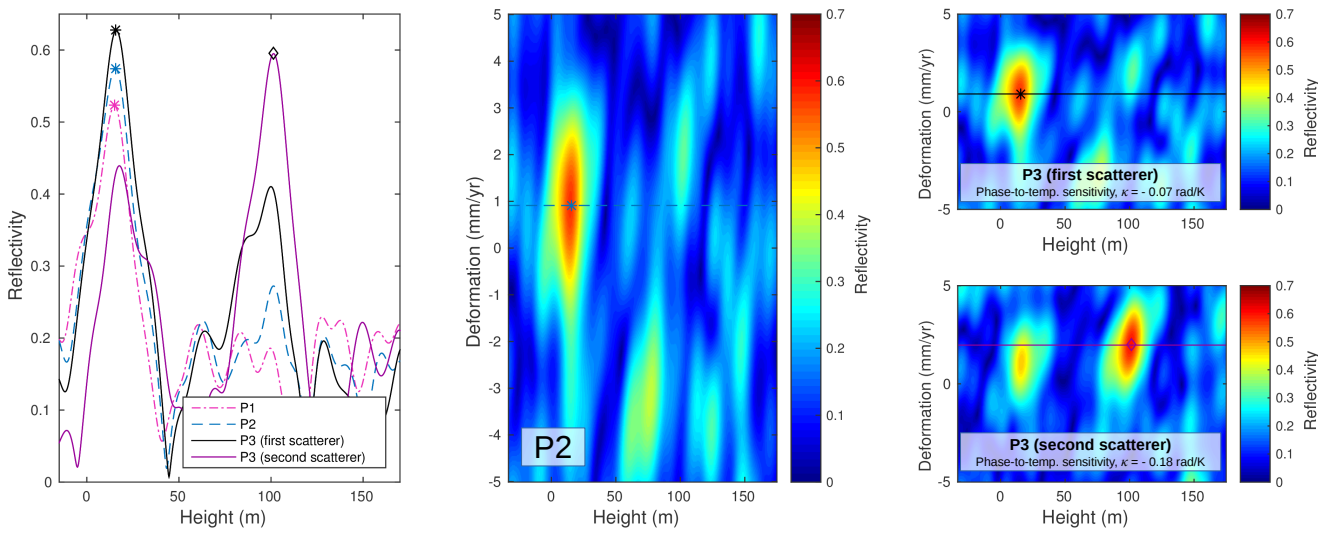


**Fig. 2**. Spatio-temporal inversion of a non-PS layover pixel (marked with a red cross in Fig. 1) using tomographic techniques. The detection/separation of double-scatterers using the extended phase model is highlighted. The first and the second scatterer are marked with * and ◊, respectively. *Left*: Elevation profiles obtained with three different phase models. *Middle*: The height-deformation plane for phase model P2 (eq. 4); the dashed-line corresponds to the elevation profile in the left figure for P2. *Right*: The height-deformation planes for phase model P3 (eq. 5): In principle, the planes are the slices of the three-dimensional (height, deformation, phase-to-temperature sensitivity) solution space at the estimated phase-to-temperature sensitivity, corresponding to the reflectivity peak, for each of the two scatterers.

$\mathcal{H}_1$ or $\mathcal{H}_0$:

$$\left(\frac{1}{N}\frac{\left|\hat{\gamma}\left(\hat{\mathbf{p}}_1\right)\right|^2}{\|\mathbf{y}\|^2}\right) \underset{\mathcal{H}_0}{\overset{\mathcal{H}_1}{\gtrless}} T_1. \tag{15}$$

## 4. RESULTS

We perform our investigations on an interferometric data stack of 50 stripmap TerraSAR-X images acquired in repeated passes over the city of Barcelona during 2007-2012. The data stack is phase calibrated within the IPTA processing. We use tomographic inversion techniques with different phase models for each pixel (whether characterized as a PS or not). To exemplify, we consider a non-PS pixel at the tip of a high-rise building, marked with a red cross in Fig. 1. The pixel is in layover. The echoes from the building tip and the roof of the nearby lower building (Diagonal Mar shopping centre) are expectedly superposed. We apply tomographic inversions with each of the three previously discussed phase models (P1, P2 and P3). The results are presented in Fig. 2. The inversion with the conventional SAR tomographic model (P1) allows only the estimation of the scatterer height (vertical projection of the estimated elevation). The height profile for P1, as shown in the Fig. 2 (left), indicates the presence of a single scatterer around 16 m. The differential tomographic phase model (P2) allows us to additionally estimate the scatterer's average deformation velocity. The height profile and the height-deformation plane for P2 also show the presence of a single scatterer. There seem to be some side-lobes in the vicinity of the detected scatterer. These results with P1 and P2 would normally be considered reasonable, as one may infer that only one of the potential two scatterers (the one corresponding to the shopping centre) is dominant. However, interestingly, the application of the extended phase model (P3) not only improves the focusing of the first scatterer, but also reveals the presence of a second scatterer corresponding to the tip of the high-rise building. The layover is resolved, and P3 has additionally provided us an estimate of the phase-to-temperature sensitivity of each of the two scatterers. In this way, tomographic inversion using the extended phase model has provided an additional deformation sample for a pixel that was originally not considered as a persistent scatterer candidate due to layover.

The tomographic inversion with P3 was applied to the entire Diagonal Mar area shown in Fig. 1. The single and double-scatterers detected with thresholds $T_1 = T_2 = 0.5$ are projected on Google Earth 3D building models, as shown in Fig. 3. Estimates of the height and deformation are also provided for each scatterer. It can be seen immediately that the estimated heights correspond fairly well with the 3D building models.

## 5. CONCLUSION & OUTLOOK

In this paper, SAR tomographic inversion has been applied in an urban area with three different phase models. A layover scenario has been analysed in detail. The results obtained emphasize that in order to achieve a reasonable tomographic inversion, an extended phase model has to be used. In addition to linear deformation over time, the extended phase model needs to account for temperature-induced scatterer motion. This is particularly true for the scatterers on high-rise buildings that are prone to thermal dilation. SAR tomography with the extended phase model effectively resolves the layover, separating the double scatterers in elevation and estimating their individual deformation parameters. Compared to our PSI solution obtained with the IPTA framework, the tomographic inversion with the extended phase model provides an increase in the deformation sampling, thereby affirming the usefulness of SAR tomography as an add-on to PSI. An assessment of the quality of the detected double-scatterers, and a consistency analysis for the estimates obtained with IPTA and tomography on scatterers commonly detected, are the subjects of our future investigations.

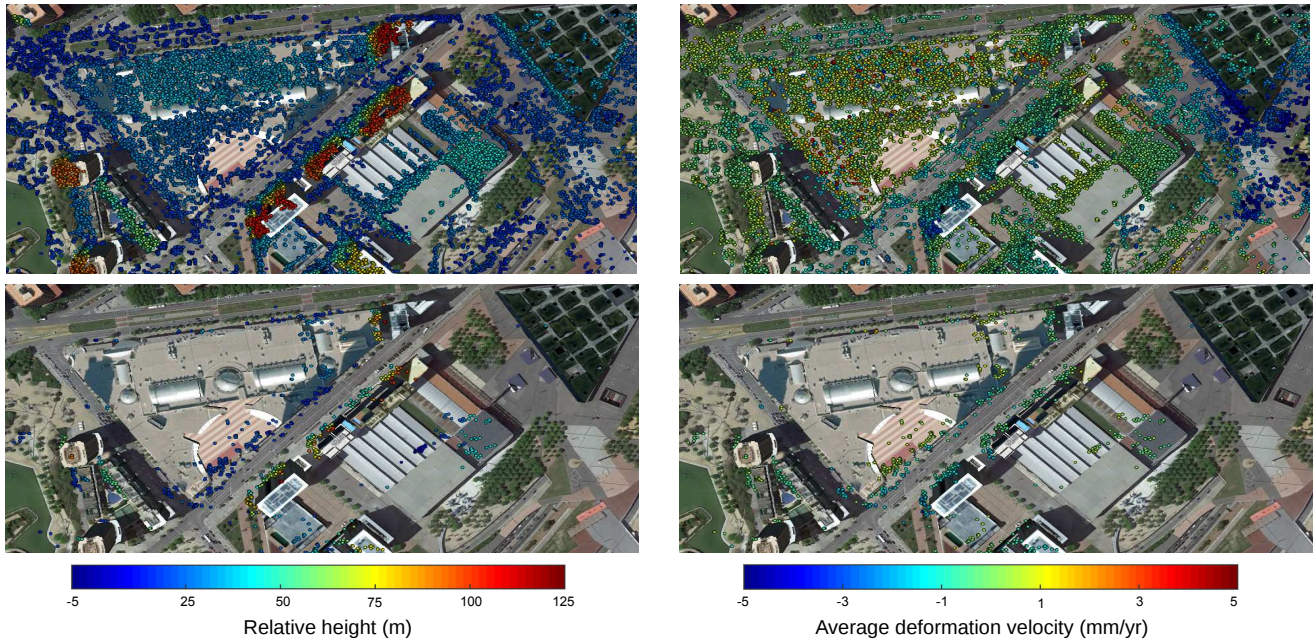


**Fig. 3**. Single (top row) and double-scatterers (bottom row) detected with tomographic inversion using the extended phase model (P3) are projected on Google Earth 3D building models. For double-scatterers, both the first and the second scatterer are shown. *Left column*: Estimated relative height (elevation projected vertically) above the datum. *Right column*: Estimated average deformation velocity.

## 6. REFERENCES


[1] A. Ferretti, C. Prati, and F. Rocca, "Permanent scatterers in SAR interferometry," *IEEE Trans. on Geosc. and Remote Sens.*, vol. 39, no. 1, pp. 8–20, 2001.

[2] C. Werner, U. Wegmüller, T. Strozzi, and A. Wiesmann, "Interferometric point target analysis for deformation mapping," in *Proc. IEEE Int. Geosci. Remote Sens. Symp.*, 2003, pp. 4362–4364.

[3] G. Fornaro and F. Serafino, "Imaging of single and double scatterers in urban areas via SAR tomography," *IEEE Trans. on Geosc. and Remote Sens.*, vol. 44, no. 12, pp. 3497–3505, 2006.

[4] X. Zhu and R. Bamler, "Very high resolution spaceborne SAR tomography in urban environment," *IEEE Trans. on Geosc. and Remote Sens.*, vol. 48, no. 12, pp. 4296–4308, 2010.

[5] F. Lombardini and M. Pardini, "Superresolution differential tomography: Experiments on identification of multiple scatterers in spaceborne SAR data," *IEEE Trans. on Geosc. and Remote Sens.*, vol. 50, no. 4, pp. 1117–1129, 2012.

[6] M. Siddique, I. Hajnsek, U. Wegmüller, and O. Frey, "Towards the integration of SAR tomography and PSI for improved deformation assessment in urban areas," in *FRINGE Workshop*, 2015.

[7] M. Siddique, I. Hajnsek, U. Wegmüller, and O. Frey, "Investigating the combined use of differential SAR tomography and PSI for spatio-temporal inversion," in *Proc. Joint Urban Remote Sens. Event*, 2015.

[8] F. Lombardini, "Differential tomography: A new framework for SAR interferometry," *IEEE Trans. on Geosc. and Remote Sens.*, vol. 43, no. 1, pp. 37–44, 2005.

[9] D. Reale, G. Fornaro, and A. Pauciullo, "Extension of 4-D SAR imaging to the monitoring of thermally dilating scatterers," *IEEE Trans. on Geosc. and Remote Sens.*, vol. 51, no. 12, pp. 5296–5306, 2013.

[10] X. Zhu and R. Bamler, "Let's do the time warp: Multicomponent nonlinear motion estimation in differential SAR tomography," *IEEE Trans. on Geosc. and Remote Sens.*, vol. 8, no. 4, pp. 735–739, 2011.

[11] O. Frey, M. Siddique, I. Hajnsek, U. Wegmüller, and C. Werner, "Combining SAR tomography and a PSI approach for high-resolution 3-D imaging of an urban area," in *Proc. 10th European Conf. on SAR*, 2014, pp. 1045–1048.

[12] A. Pauciullo, D. Reale, A. De Maio, and G. Fornaro, "Detection of double scatterers in SAR tomography," *IEEE Trans. on Geosc. and Remote Sens.*, vol. 50, no. 9, pp. 3567–3586, 2012.

[13] U. Wegmuller and C. Werner, "Mitigation of thermal expansion phase in persistent scatterer interferometry in an urban environment," in *Proc. Joint Urban Remote Sens. Event*, 2015.

[14] X. Zhu and R. Bamler, "Compressive sensing for high resolution differential SAR tomography - the SL1MMER algorithm," in *Proc. IEEE Int. Geosci. Remote Sens. Symp.*, 2010, pp. 17–20.

[15] O. Monserrat, M. Crosetto, M. Cuevas, and B. Crippa, "The thermal expansion component of persistent scatterer interferometry observations," *IEEE Trans. on Geosc. and Remote Sens.*, vol. 8, no. 5, pp. 864–868, 2011.

[16] O. Frey, I. Hajnsek, U. Wegmüller, and C. Werner, " SAR tomography based 3-d point cloud extraction of point-like scatterers in urban areas," in *Proc. IEEE Int. Geosci. Remote Sens. Symp.*, 2014, pp. 1313–1316.